Electrochemical behavior of membrane based on zirconium (IV) phosphoborate nanocomposite and its application in dye removal

Name(s) of the Author(s) and Affiliation(s):

Sandeep Kaushal[1], Rahul Badru[1*], Sanjeev Kumar[2], Pushpender K Sharma[3], Susheel K Mittal[4] and Pritpal Singh[1*]

[1]Department of Chemistry, Sri Guru Granth Sahib World University, Fatehgarh Sahib (Pb), India.

[2]Department of Physics, Sri Guru Granth Sahib World University, Fatehgarh Sahib (Pb), India

[3]Department of Biotechnology, Sri Guru Granth Sahib World University, Fatehgarh Sahib (Pb), India

[4]School of Chemistry & Biochemistry, Thapar University, Patiala 147004, India

Address for Correspondence:

Dr. Pritpal Singh

Associate Professor and Head,

Department of Chemistry,

Sri Guru Granth Sahib World University, Fatehgarh Sahib (Pb), India.

Mobile No: +91-84270-00415

Fax: +91-1763-234236,   Email: dhillonps2003@gmail.com

&

Dr. Rahul Badru

Assistant Professor

Department of Chemistry,

Sri Guru Granth Sahib World University, Fatehgarh Sahib (Pb), India.

Mobile No: +91-9988479134

Fax: +91-1763-234236,   Email: rahulbadru@gmail.com

Abstract: A new hybrid ion-exchange membrane was prepared from novel composite obtained by dispersion of polyaniline into inorganic matrix of zirconium (IV) phosphoborate employing sol-gel method. The composite was characterized by FTIR, XRD, SEM, TEM and TGA/DTA analysis. Membrane potential, transport number, permselectivity and fixed charge density were studied as a function of electrolytic concentration, in order to explore the electrochemical behavior of prepared membrane. Values for all these electrochemical properties were found to increase upto a mean concentration for each electrolyte and declined thereafter. All these electrochemical properties possess higher values for monovalent alkali metal cations than those for bivalent alkaline earth metal cations. The nanocomposite worked well to hamper the growth of both G^- and G^+ bacterial cultures of Escherichia Coli and Bacillus strains to a remarkable level. The nanocomposite was also evaluated for adsorptive removal of methylene blue from aqueous solutions. Maximum adsorption was achieved at pH 11 with adsorbent dosage of 20 mg for 1.6 mg/100 ml dye solution in an interval of 3.5 hrs. Upto 99% dye was recovered upon elution and regenerated column was efficiently used a number of times. Promising results obtained in dye removal by adsorption and antimicrobial activity encourage the use of such composites in water purification.

Key words: Nanocomposite; Polyaniline; methylene blue; adsorption; antimicrobial; zirconium phosphoborate

1. Introduction

Inorganic ion exchangers have been comprehensively used in pollution control, sensors, separation of radioisotopes and water purification [1]. The low mechanical and chemical stability of these ion exchangers are the main constraints. In addition, fine powdered form makes them unsuitable for column operations. The low pollutant removal capacity and less stability in high radiation fields are the major drawbacks of organic ion exchangers which make them unsuitable as alternative of inorganic exchangers [2]. The hybrid (organic-inorganic) nano composite ion-exchangers prepared by various methods are advanced materials which have attracted a good deal of attention [3] due to their stability and reproducible analytical and electroanalytical applications. The specificity, selectivity and extensive range of applicability of nano domain advanced composite ion exchangers have made them most promising agents for environmental remediation. Recently, Yao et al and Bradder et al have reported the use of ferric oxide and graphene oxide nanoparticles based nanocomposites in waste water remediation via adsorptive removal of dyes on the composite surface [4]. Adsorption is gaining much more attention in water remediation over other conventional techniques as it possesses advantageous features of easy mode of operation, low cost and versatility without need of any highly sophisticated instrument [5]. Although the hybrid nano-composites are advancing in waste water remediation through adsorption now a days [6], but increasing toxicity of water due to discharge of synthetic organic dyes by textile and paper industries still demands the development of efficient and low cost adsorptive composite materials that can sustain water for future use. In present work, polyaniline (PANI) doped zirconium phosphoborate (ZrPB) nanocomposite has been synthesized by sol-gel method. The composite has been used to fabricate a membrane in order to explore the electrochemical properties like membrane potential, transport number, permselectivity and fixed charge density. The real life application of nanocomposite has also been explored by employing it in adsorptive removal of methylene-blue dye from aqueous solution and as antibacterial agent against Escherichia Coli and Bacillus strains of bacteria.

PANI was selected as the organic matrix as it is a low cost conducting polymer with suitable biological and chemical resistance [7]. Among various inorganic ion exchangers, ZrPB is matter of choice as it is reported to be an excellent ion exchanger with better electrochemical properties [8]. Till date, none of the papers reports the doping of PANI into zirconium phosphoborate inorganic matrix, although a few publications report incorporation of PANI into

other similar inorganic matrix [9]. A detailed electrochemical characterization of IEMs prepared using PANI is still desirable.

2. Experimental

2.1. Reagents and Instruments

The reagents used for synthesis were of analytical grade and used as received, without any further purification. Thermal analysis was performed by heating nanocomposite material up to 700°C at a constant increment of 10°C per minute in nitrogen atmosphere, using Hitachi SGA7400 thermogravimetric analyzer. IR spectra were recorded on a Perkin Elmer RX I FTIR spectrophotometer. X-ray diffraction patterns were obtained using PAN analytical system DY 3190 X-ray diffractometer. The spectrum was recorded between 5° to 40° at 2θ, using Cu Kα radiation. The topography and elemental composition of the synthesized particles were recorded using JEOL scanning electron microscope and JSM 6510LV energy dispersive X-ray detector. Transmission electron microscopy (TEM) studies were done using model MIC JEM 2100. Potentiometric studies were done on Systronic digital potentiometer (model 318). Elico pH meter (model 1012) was employed to perform pH studies. Membrane thickness was measured using screw gauge.

2.2. Preparation of Nanocomposite

2.2.1. Preparation of ZrPB

Boric acid and phosphoric acid solutions (250 mL of 0.1 M each) were mixed in a round bottom flask and heated to 60°C using heating mantle. The assembly was fitted with mechanical stirrer and 500 mL of 0.1 M zirconyl oxychloride solution was added to the mixture in a period of half an hour with continuous stirring while maintaining the temperature at 60°C. The gel thus formed was permitted to stand overnight. The gel was repeatedly washed with distilled water to remove chloride ions.

2.2.2. Preparation of PANI

10% aniline solution (v/v) was prepared in 1M HCl solution and placed under ice-cold conditions to maintain the temperature below 10°C. Ice cold potassium persulphate solution (0.1 M) was added in fractions, to a continuously stirred solution of aniline (10% v/v) in 1:1 volume ratio, maintaining the pH ~1 [9]. Appearance of green colour from the initial brown colour

indicated the completion of reaction. Stirring was further continued for 30 minutes. The polyaniline gel obtained was used as such for the next step.

2.2.3. Preparation of PANI-ZrPB Nanocomposite

Green gel of PANI was introduced into the ZrPB gel and the mixture was refluxed at room temperature for 2 hrs using mechanical stirrer. The composite was filtered under suction and washed with distilled water to remove the unreacted part. The gel was then dried in an air oven at 40°C. Five samples (S1-S5) were prepared by varying the mixing volume ratio of polyaniline and zirconium phosphoborate.

2.3. Ion-exchange capacity (IEC)

The ion exchange capacity of the dry PANI-ZrPB nanocomposite ion-exchanger in H^+ form was determined by column method, using sodium nitrate solution (0.1 M) as an eluent. H^+ ions eluted from the column were determined titrimetrically against standard solution of sodium hydroxide. Ion exchange capacity (IEC) was calculated by the formula:

$$IEC = \frac{N \times V}{W} \, meq/g$$

where N and V are normality and volume in ml of NaOH, respectively, and w is weight in gram of PANI-ZrPB nanocomposite.

2.4. Membrane Preparation

The nanocomposite was ground to a fine powder (approximately 200 micrometer in a sieve), and then mixed thoroughly with araldite [PANI-ZrPB: epoxy resin = 80:20 (w/w)]. The slurry was spread between the folds of a glossy paper and a pressure of 2.0 Kg/cm^2 was applied over the glass plates containing the glossy paper for 24 hours. The glossy paper was removed by dipping the membrane in distilled water. Circular membranes were obtained by cutting with sharp knife.

2.5 Physical Characterization of fabricated nanocomposite membrane
2.5.1. Thickness
The thickness of the membrane was measured by a screw gauge. The difference between the average thickness of the membrane equilibrated with 1 M NaCl for 24 h and the dry membrane is a measure of swelling.

2.5.2. Porosity (ε)

Porosity is regarded as the volume of water incorporated in the cavities per unit membrane volume and calculated from the following relation:

$$\varepsilon = \frac{m_w - m_d}{AL\rho_w}$$

where m_w and m_d are the mass (g) of wet and dry membrane, respectively. L is the thickness of the membrane, A is the area of the membrane, and ρ_w is the density of water.

2.5.3. Water uptake of membranes

The water content was measured as the weight difference between the dried and swollen membranes. The wet membrane was weighed and then dried in oven until a constant weight was obtained. Following equation can be used in water content calculations:

Water content (%) = $\dfrac{W_{wet} - W_{dry}}{W_{dry}} \times 100$

Where W_{wet} and W_{dry} are the masses in gram of the wet membrane and the dry membrane, respectively.

2.6. Electrochemical properties of fabricated nanocomposite membrane

2.6.1. Electrode Assembly

Membrane potential measurements were made using saturated calomel electrodes as reference electrodes.

$$Hg \mid Hg_2Cl_2, Cl^- \parallel \text{solution } C_1 \mid \text{Membrane} \mid \text{solution } C_2 \parallel Cl^-, Hg_2Cl_2 \text{ (s)} \mid Hg$$

Potential measurements were made for different concentrations of same electrolyte on two sides of the membrane in such a way that the concentration ratio $\delta(C_2/C_1)$ is 10. During measurements, the electrode assembly was kept immersed in water thermostat maintained at $27\pm0.1^\circ C$.

2.6.2. Membrane potential and transport number

The potential difference developed across the membrane was measured against Hg-Hg_2Cl_2, Cl^- reference electrode on either side of the membrane, using a digital potentiometer. The electrode chambers were rinsed with electrolyte solution of next higher concentration and then filled with the same solution. The membrane was allowed to equilibrate for 2 hours and the new potential

difference was then noted. The membrane potential measurements were reproducible to $\pm$ 0.1 mV.

The transport number $\bar{t}_+$ was calculated by the following equation [11]:

$$E_m = 2.303 \frac{RT}{nF}(2\bar{t}_+ - 1)\log\frac{C_2}{C_1}$$

where, R is gas constant, F is Faraday constant, T is absolute temperature, C_1 & C_2 are the concentrations of electrolyte solution in the test cell.

2.6.3. Permselectivity

The ionic selectivity of membrane is expressed quantitatively in terms of membrane permselectivity, based on migration of counter ions through cation exchange membrane [12].

$$P_s = (\bar{t}_+ - t_+)/(1 - t_+)$$

Where P_s is the permselectivity of the membrane, $\bar{t}_+$ and t_+ refer to the transport numbers of counter ion in the membrane and in free solution at the same concentration, respectively [13].

2.6.4. Fixed charge density ($\overline{X}$)

The electrical character of a membrane is expressed in terms of fixed charge density. The fixed charge density of the prepared membrane for 1:1 and 1:2 electrolytes has been evaluated by Kobatake equation [14].

$$E_m = -\frac{RT}{F}[\frac{1}{\beta}\ln\frac{C_2}{C_1} - (1 + \frac{1}{\beta} - 2\alpha)\ln\frac{C_2 + \alpha\beta\,\overline{X}}{C_1 + \alpha\beta\,\overline{X}}]$$

Where $\alpha = \dfrac{u}{u+v}$ & $\beta = 1 + \dfrac{KF\overline{X}}{u}$

Where E_m is membrane potential difference; u & v are ionic mobilities of cation and anion, respectively; K is a constant depending on the solution viscosity and F is Faraday constant.

2.7. Antibacterial Study

The antibacterial effects of inorganic part (ZrPB), organic part (PANI) and hybrid nanocomposite (PANI-ZrPB) were investigated individually. Initially, the cultures for both the *E. coli* and *Bacillus* were grown overnight aseptically, in an incubator maintained at 37°C with a

shaking speed of 220 rpm. The 1% overnight grown culture was transferred to new flasks having 20 milliliter Luria Broth. A control experiment was set for both *E. coli* and *Bacillus* without the addition of any chemical. In another control experiment, 500 µl DMSO (dimethyl sulfoxide) was added into each *E. coli* and *Bacillus* culture. In the test experiments, all chemical agents *viz.* inorganic part, organic part and nano-composite were added at final concentration of 50µg in each of the six flasks. Following one hour of growth in shaker, one milliliter culture was withdrawn from respective flask at an interval of two hours. The optical density (OD_{600nm}) was recorded for each sample and OD_{600nm} versus time (h) graph was plotted to measure the rate of growth inhibition.

2.8. Adsorption studies

A series of volumetric flasks of 100 mL capacity containing 25 mL of adsorbate solution of different concentrations were prepared. The pH of the solution was adjusted by addition of 1% NaOH solution. Ion exchange composite material (20 mg) was then added as adsorbent in each flask. The solution was stirred for 4 hours employing magnetic stirrer. The filtrate was analyzed for final concentration of the dye by measuring the absorbance.

2.9. Column studies

Fixed bed adsorbent columns of the synthesized nanocomposite were prepared to find the percentage removal of adsorbed dye and to check the reusability of spent column. A specific amount of nanocomposite was added to the glass column [30 cm length and 1 cm internal diameter]. Adsorbate solution of known concentration was percolated through the column at a constant flow rate of 0.5 mL min^{-1}. In each case, 10 mL aliquots of effluents were collected and the effluent concentration was analysed spectrophotometrically. Regeneration and recovery of the adsorbent was also performed on the exhausted column by elution with 10% HCl solution.

3. Results and Discussion

To meet the requirements of synthesizing an electro-active material that possesses better transport number, permselectivity, fixed charge density and ion-exchange phenomenon than the already reported ZrPB inorganic component, five different samples (**S1-S5**, **Table 1**) were prepared by varying the volume ratio of inorganic exchanger, aniline and potassium persulphate. All the samples of nanocomposite possessed enhanced IEC for Na^{+} ions than its inorganic

counterpart ZrPB under identical conditions. The binding of organic material (PANI) into the inorganic matrix may account for the increased IEC of nanocomposite over the inorganic counterpart ZrPB under identical conditions [6c]. The organic part also enhances the mechanical strength and surface area of the nanocomposite material [15]. Since IEC provides information about charge density in the membrane, so it was selected as preliminary criteria that decides the other electrochemical parameters like transport number, permselectivity and fixed charge density in one way or the other. So, the sample with maximum IEC of 0.67 meqg^{-1} for Na^{+} ion (Sample **S-4**, **Table 1**) in comparison to an IEC of 0.38 meq g^{-1} of ZrPB [8], was selected for fabrication of membrane. The prepared nanocomposite has been characterized through FESEM, EDX, TEM, FTIR, and TGA studies.

3.1. Structural and morphological characterization of PANI-ZrPB composite

3.1.1. FTIR studies

The incorporation of organic polymer PANI into the inorganic matrix ZrPB has been confirmed by carrying out IR studies. Peaks at 3560, 3458, 3011, 1604 and 1500 cm^{-1} in the FTIR spectrum of PANI-ZrPB nanocomposite (**Fig. 1**) correspond to organic counterpart, while peaks at 1025, 813, 756 and 640 cm^{-1} correspond to inorganic ion exchanger. Peak at 3011 cm^{-1} is due to aromatic C-H stretching, whereas peaks at 3560 cm^{-1} and 3458 cm^{-1} may be assigned to O-H and N-H stretching vibrations, respectively. Despite benzenoid ring stretching at 1500 cm^{-1} [16], peaks at 1604 and 1220 cm^{-1} correspond to N-H bending and C-N stretching, respectively in the neighbourhood of a quinoid ring [17]. Ionic phosphate stretching appears at 1025 cm^{-1} [18]. Peaks at 813, 756 and 640 cm^{-1} may be assigned to M-O stretching [19].

3.1.2. X-ray diffraction studies

Narrow width of peaks in the X-ray diffraction pattern indicates the crystalline nature of synthesized composite. The diffraction pattern (**Fig. 2**) further reveals that the sample exhibits characteristic peaks of PANI–ZrPB composite which are well matched with JCPDS card numbers 39-1893 and 23-0063, thus confirming the crystalline nature of sample.

3.1.3. FESEM and EDX studies

Fig. 3a and 3b show the FESEM micrographs of ZrPB and PANI-ZrPB nanocomposite, respectively. FESEM micrograph (**Fig. 3a**) taken at 2,50,000X shows the agglomerates and

aggregates of ZrPB particles. The particles are found to be quasi spherical (spherical marked in **Fig. 3a**) and further form the clusters (marked region P). The nanosize of the ZrPB particles has been confirmed from 500 nm scale bar on the micrograph. **Fig. 3b** shows the aggregates of the PANI-ZrPB composite taken at 2,00,000X. The cluster size of the PANI-ZrPB composite is larger as compared to ZrPB (marked regions in **Fig. 3b**). It is clearly revealed from the micrographs that after binding of PANI with ZrPB, the topography of the ZrPB has changed. EDX spectrum of PANI-ZrPB nanocomposite (**Fig. 3c**) confirms the presence of Zr, P, B, C, O, N.

3.1.4. TEM studies

TEM image of ZrPB particles taken at 3,00,000X (**Fig. 4a**) shows the homogenous distribution of nearly spherical particles. The 20nm scale bar in the image confirms the nanometer size of the ZrPB particles. The size of ZrPB particles varies from 2-6 nm range with average size of 4 nm (**Fig. 4c**), histogram of size variation). **Fig. 4b** shows the TEM image of PANI-ZrPB composite taken at 2,00,000X. It shows the aggregation in-between PANI-ZrPB composites. The nanosize of the composite has been confirmed by comparing the particle size with 100nm scale bar in the image. PANI has a great influence on the morphology of ZrPB. The image depicts the morphological changes i.e. from spherical to rod shape, which occurred after binding of inorganic precipitate with the organic polymer matrix. These morphological changes are also reflected in the SEM micrograph of the composite.

3.1.5. TGA/DTA Studies

The TGA/DTA studies of PANI-ZrPB nanocomposite are shown in **Fig. 5**. The nanocomposite exchanger was heated from room temperature to 700°C, with an increment of 10 °C/min in air. The weight loss reflected by TGA in temperature range from 110-170°C corresponds to exothermic hump in the same region in the DTA curve, and this weight loss (18.0%) may be due to evaporation of water molecules from the sample [20]. Similarly, there is an exothermic hump in the region 280-310 °C, which corresponds to weight loss (10.1%) shown by TGA curve in the same region. This may be due to conversion of some phosphate into pyrophosphate [21]. The last exothermic hump observed in temperature range from 380-430 °C corresponds to weight loss of 6.1% in TGA curve. Further loss above 430 °C temperature may

be assigned to loss of organic component (degradation of oligomeric and polymeric chains at higher temperature) [22] from the nanocomposite material.

3.2. Membrane Preparation and Physiochemical Characterization

The nanocomposite was ground to a fine powder (approximately 200μm). Araldite and the nanocomposite were mixed in the ratios 1:9, 2:8 and 3:7 for fabrication of three membranes of different compositions. An ideal membrane should have less thickness, moderate porosity and water content and high ion exchange capacity. It can be seen from **Table 2** that the water content and ion exchange capacity of the membrane decreased with increasing thickness of the prepared membranes. Membrane M-2 was selected for electrochemical studies due to its better ion exchange capacity than membrane M-3. Membrane M-1 having even higher ion exchange capacity than M-2 was not selected for further studies as it was too thin to work, and suffered from frequent leakage during experiments.

3.3. Electrochemical studies of PANI-ZrPB nanocomposite for different electrolytes

3.3.1. Membrane potential

Membrane potential values increased with the increase in concentration for each electrolyte (**Fig. 6a**) up to a mean electrolyte concentration of 0.06 M. This may be due to the improved ion transportation through the suitable flow channels provided by nanocomposite with increasing concentration of the electrolyte. Thereafter, the values of membrane potential tend to decline. This may be attributed to the compression of electrochemical double layers on the membrane surface [23] and concentration polarization phenomenon at high concentration, resulting in increased co-ion percolation.

3.3.2. Transport Number and Permselectivity

The transport numbers can be calculated from membrane potentials which develop when the membrane separates electrolyte solutions of unequal concentrations. The membrane consisting of the ion exchange material (PANI-ZrPB) embedded in an inert matrix of adhesive (Araldite) separates electrolyte solutions of different concentrations. Due to natural tendency, the electrolyte in concentrated compartment moves towards the dilute solution through the ion exchange membrane containing more labile hydronium ions which facilitate the transport by ion exchange with the counter ions. The ion exchange membrane then offloads the counter ions in

the dilute solution compartment. The movement of cations from the concentrated electrolyte towards the dilute electrolyte is driven by a resultant loss of free energy from the system.

The transport number (mobility) of the electrolyte in membrane phase increases with increase in concentration upto a certain limit for all the electrolytes (**Fig. 6b**). A gradual drop in the values was observed with further increase in concentration of electrolyte. The increase in transport numbers initially, may be attributed to increase in the number of cations (counter ions) available for transport with increase in concentration of the electrolyte. With further increase in concentration of electrolyte beyond a certain limit, increased inter-ionic interactions and concentration polarization phenomenon lead to lower values of transport numbers. The permselectivity exhibits the same trend as that of transport numbers (**Fig. 7**). Fall in permselectivity with increasing concentration of electrolyte is also supported by the Donnan exclusion principle [24].

The ion selectivity of ion exchange membranes is quantitatively expressed in terms of membrane permselectivity, which measures the ease with which the counter ions migrate through an ion exchange membrane. The membrane potentials, transport numbers (**Fig. 6a,b**) and permselectivity (**Fig. 7**) of the membrane for monovalent alkali metal cations were found to be higher than those for bivalent alkaline earth metal cations. It may be due to stronger electrostatic interactions of bivalent cations with fixed ion exchange functional groups on the ion exchange membrane [25]. Moreover, the bivalent cations have larger hydrated ionic radii as compared to monovalent cations, leading to their lesser penetration into the membrane. Among the alkali metal and alkaline earth metal ions, potassium (I) and barium (II) ions, respectively, have higher values of membrane potential owing to their smallest hydrated ionic radii in their respective groups.

3.3.3. Fixed Charge Density

The nature of fixed charge in the membrane matrix greatly influences the counter-ion than the co-ion, as well as the transport phenomenon. The observed values of fixed charge density indicate that larger part of internal fixed charge is active. It may be due to the reason that active fixed charges in the membrane are essentially those on the surface of nanocomposite cation exchanger. The higher fixed charge density of the membrane for potassium ions (**Fig. 8**) is attributed to its smaller hydrated ionic radius. The trend of electrochemical properties of the

membrane confirmed that the membrane is highly selective for K^+ ions among alkali and alkaline earth metal cations.

3.4. Antibacterial studies on PANI-ZrPB nanocomposite

Investigation of the antibacterial activity revealed that all compounds *viz* ZrPB, PANI, PANI-ZrPB were able to hamper the growth of both G^- and G^+ bacterial culture to a remarkable level. The control experiments however demonstrated normal growth. Interestingly, the inhibitory effect was observed in the order ZrPB< PANI <ZrPB-PANI, and was increasing with time as depicted in **Fig. 9**.

The nano-composite particles having ~30 nm size (as validated by TEM) can easily interact with the cell membrane and may disrupt the cellular and molecular functions of the cell, primarily by interfering with its permeability. Similar observations were reported previously where the nano size particles of composite were suggested to be interfering with the cellular and molecular machinery of the cell [26]. Recently Li et al [27] also reported similar antibacterial effects of silver nano particles. Their study has shown that the nanoparticles may enter the inner bacterial membrane and can inactivate number of respiratory enzymes that may result in retardation of normal growth of the cells. This may finally result in collapsing of membrane structure that eventually causes death of cells. The preferred selectivity of the nano composite exchanger towards K^+ ion (**Fig. 8**) substantiates our observation of enhanced antibacterial effects in presence of exchanger as K^+ ions are involved in membrane transport under heading Na^+-K^+ pump [28]. It can be hypothesized that K^+ ions may impair the permeability processes across the membrane and may further retard the bacterial growth.

3.5. Adsorption studies of methylene blue over PANI-ZrPB nanocomposite

Preliminary studies like the effect of pH, adsorbent dosage and contact time were performed before carrying out batch adsorption of methylene blue dye from aqueous solutions over nanocomposite surface.

The adsorption conditions were optimized to obtain maximum adsorption of methylene blue over nanocomposite surface and results are reported in **Table 3**. The results indicate that the extent of adsorption of the dye increased rapidly with increasing pH from 3 to 11 (**Table 3,** 1-9) and thereafter decreases or remains constant. The higher adsorption of the dye at high pH is apparently due to the effect of pH on surface binding sites of the adsorbent, and on the ionization

process of the dye molecules. This leads to greater accessibility of the dye to the active sites. An optimum pH of 11 was selected for further investigations as the nanocomposite reflected maximum adsorption at this pH value.

As expected, the percentage of dye adsorption increased with increasing adsorbent dosage at the same initial dye concentration in all cases [**Table 3,** 9-13]. The increase in dye removal with the adsorbent dose can be attributed to the increased surface area and the adsorption sites. Optimum dosage of nanocomposite for dye removal has been observed to be 20 mg as no significant change was observed with further increase in the amount of adsorbent.

The contact time required for establishment of equilibrium suggests the effectiveness of the composite employed for wastewater treatment. In order to determine the equilibrium time for maximum dye uptake, percentage adsorption was recorded at different time intervals with a fixed adsorbent dose of 20 mg added to 1.6 mg/100 ml (**Table 3,** 10,14-17) dye solution at pH 11. After one, two and three hours of contact, about 40.5%, 66.6% and 84.3% of the dye was adsorbed, respectively. Results reflect that the adsorption reaches maximum value of 92.5% in three and half hours, and attains a saturation value with further increase in time.

3.5.1. Adsorption isotherms

Successful application of the adsorption technique demands studies based on various adsorption isotherm models. The adsorption isotherm models clearly depict the relationship of amount adsorbed by a unit weight of adsorbent with the concentration of adsorbate remaining in the solution at equilibrium. Thus, Freundlich and Langmuir models were applied to the experimental data.

Langmuir isotherm

The Langmuir isotherm assumes that the surface of any adsorbent material contains a fixed number of active sites and saturation of these active sites stops further adsorption of the adsorbate. This indicates that the adsorption occurs until a monolayer of adsorption is completed and no further adsorption occurs at that site. The equation is stated as:

$$\frac{1}{q_e} = \frac{1}{Q_0} + \frac{1}{bQ_0C_e}$$

Where q_e is the amount adsorbed (in mol g^{-1}), C_e denotes the equilibrium concentration of the dye (in mol L^{-1}), Q_o is the adsorption capacity (mol g^{-1}), and b is the energy of adsorption (L mol^{-1}). Straight line obtained between $1/q_e$ and $1/C_e$ (**Fig. 10a**) shows that the adsorption data fits into Langmuir adsorption isotherm. Langmuir constants can be calculated from the plot.

Freundlich isotherm

The Freundlich model is based on the assumption that adsorption occurs on a heterogeneous adsorption surface having unequally available sites with different energies of adsorption and is

given by the relation: $\log q_e = \log K_F + \dfrac{1}{n}\log C_e$; where q_e is the amount adsorbed (mol g^{-1}), and

C_e is the equilibrium concentration of the adsorbate (mol L^{-1}). The plot of log q_e with log C_e for the nanocomposite adsorbent along with R^2 value is presented in **Fig. 10b**. Straight line obtained for the Freundlich isotherm models was used to calculate different Freundlich constants.

3.5.2. Desorption of dye and reusability of nanocomposite

The spent column was eluted with 10% HCl solution (pH 1) under fixed flow rate of 8-10 drops per minute, for recovery of the dye and regeneration of the column. The column was washed with distilled water after elution with10% HCl solution, dried and re-employed in dye adsorption to check its reusability. The percentage adsorption of the dye for first, second, third, fourth and fifth batch was found to be 95.1%, 92.3%, 90.6%, 86.23% and 81.9%, respectively. The percentage recovery of the dye on elution was 99.0%, 92.3%, 90.6%, 86.2% and 78.2% for first, second, third, fourth and fifth batch, respectively (**Fig. 11**).

Conclusions

In summary, the prepared polyaniline doped zirconium phosphoborate nanocomposite featured to be a better ion exchange material than its inorganic counterpart zirconium phosphoborate. The membrane potential, transport number and permselectivity values studied with the membrane fabricated from the composite were found to be higher for monovalent cations than those for bivalent cations. The nanocomposite worked well to hamper the growth of both G^- and G^+ bacterial cultures of Escherichia Coli and Bacillus strains to a remarkable level. The nanocomposite was also evaluated for adsorptive removal of methylene blue from aqueous

solutions. Remarkable results obtained in dye removal by adsorption and antimicrobial activity encourage the use of such nanocomposites in water purification for environmental remediation.

References

1. a) S.A. Nabi, S.A. Ganai, A.M. Khan, J. Inorg. Oranomet. Polym., 21 (2011) 25-35; b) T. Liang, C. Hsu, Radiochim. Acta, 61 (1993) 105-108; c) H. Lopez, M.T. Olguin, P. Bosch, S. Bulbulian, J. Radioanl, Nucl. Chem. Lett., 200(1) (1995) 19-23.

2. a) W.A. Siddiqui, S.A. Khan, Inamuddin, Colloids Surf. A, 295 (2007) 193-199; b) R. Niwas, A.A. Khan, K.G. Varshney, Colloids Surf. A, 150 (1999) 7-14.

3. a) K.G. Varshney, N. Tayal, A.A. Khan, R. Niwas, Coll. Surf. A: Physicochem. Eng. Aspects 181 (2001) 123-129; b) K.G. Varshney, N. Tayal, Langmuir 25 (2001) 89-93; c) K.G. Varshney, P. Gupta, Indian J. Chem., 42A (2003) 2974-2977; d) A. A. Khan, M. M. Alam, Inamuddin, Mater. Res. Bull., 40 (2005) 289-305; e) M.D. A. Khan, A. Akhtar, S. A. Nabi, M. A. Khan, Ind. Eng. Chem. Res., 53 (2014)15253; f) S. Kaushal, R. Badru, S. Kumar, S. Mittal, P. Singh, RSC Adv., 6(2016) 3150-3158.

4. a)Y.S. Yao, Miao, S. Liu, P. Li, H. Sun, S. Wang, Chem. Eng. J., 184 (2012) 326–332; b) P. Bradder, S. Ling, S. Wang, S. Liu, J. Chem. Eng. Datam 56 (2011) 138–141.

5. K. E. Noll, G. Vassilios, W.S. Hou, Adsorption Technology for Air and Water Pollution Control, Lewis Publishers, Chelsea, MI, USA, 1992.

6. a) V. K. Gupta, S. Agarwal, I. Tyagi, D. Pathania, B. S. Rathore, G. Sharma, Ionics, 21 (7) (2015) 2069-2078; b) G Sharma, D Pathania, Mu. Naushad, Ionics, 21 (2015) 1045-1055; c) G. Sharma, D. Pathania, Mu.Naushad, N.C. Kothiyal, Chem. Eng. J., 251 (2014)413-421.

7. V. K. Gupta, D. Pathania, N. C. Kothiyal, G. Sharma, J. Mol. Liq., 190 (2014) 139-44.

8. a) P. S. Thind, S. K. Mittal, S. Gujral, Synth. React. Inorg. Met. Org. Chem., 18 (1988) 593-607; b) S. Kaushal, P. P. Singh, S. K. Mittal, J. Electro. Sci. Eng., 4 (2014) 55-65.

9. a) Z. A. Alothman, M. M. Alam, M. Naushad, R. Bushra, Int. J. Electrochem. Sci., 10 (2015)2663-2684; b) A. A. Khan, S. Shaheen, J. Electroanl. Chem., 714-15 (2014) 38-44; c) S. A. Nabi, Mu. Naushad, J. Colloids Surfaces A: Physical Engineering Aspects, 316 (2008) 217-225.

10. Z. Alam, Inamuddin, S. A. Nabi, Desalination., 250 (2010) 515-522.

11. N. Lakshiminarayanaiah, Transport phenomena in membranes, Academic Press, New York, 1969.

12. a) G. S. Gohil, V. V. Binsu, V. K. Shahi, J. Membr. Sci., 280 (2006) 210–218; b) R. K. Nagarale, V. K. Shahi, S. K. Thampy, R. Rangarajan, React. Funct. Polym., 61 (2004) 131–38.

13. D. R. Lide, CRC press, Taylor & Francis Group, Florida (2006-2007).

14. Y. Kobatake, N. T. Toyoshima, H. Futiza, J. Phys. Chem., 69 (1965) 3981-3988.

15. G. Crinic, Bioresour. Technol., 97(2006)1061-85.

16. Y. Furukawa, F. Ueda, Y. Hyodo, I. Harada, T. Nakajima and T. Kawagoe, Macromolecules, 1988, 21, 1297; (b) Z. Ping, J. Chem. Soc., Faraday Trans., 1996, 92, 3063.

17. E. T. Kang, K. G. Neoh and K. L. Tan, Prog. Polym. Sci., 1998, 23, 277.

18. a) C. N. R. Rao, Chemical Applications of Infrared Spectroscopy, Academic Press, New York, 1963, p. 53; (b) V. K. Gupta, D. Pathania, N. C. Kothiyal and G. Sharma, J. Mol. Liq., 2014, 190, 139–145.

19. G. Socrstes, Infrared Characteristics Group Frequencies, Wiley, NJ, 1980, p. 145.

20. C. Duval, Inorganic Thermogravimetric Analysis, 2nd edition, Elsevier, Amsterdam, 1963.

21. S. A. Innamuddin, A. A. Siddiqui, A. A. Khan. 2007. Synthesis, characterization and ion-exchange properties of a new and novel 'organic–inorganic' hybrid cation-exchanger: Nylon-6,6, Zr(IV) phosphate, Talanta, 71:841- 47.

22. Y. Kobatake, N. T. Toyoshima, H. Futiza, J. Phys. Chem. 69 (1965) 3981-3988.

23. K. Singh, A. K. Tiwari, Proc. Ind. Natl. Sci. Acad. ,70A (2004) 477-84.

24. S. M. Hosseini, S. S. Madaeni, A. R. Khodabakhshi, Sep. Sci. Technol., 45 (2010) 2308-2321.

25. R. K. Nagarale, G. S. Gohil, V. K. Shahi, R. Rangarajan, Colloids Surf. A, 251 (2004) 133-140.

26. E. M. Grainger, H. S. Kim, J. P. Monk, S. A. Lemeshow, M. Gong, R. R. Bahnson, S. K. Clinton, Uro. Oncol., 26 (2008) 125-32

27. W. R. Li, X. B. Xie, Q. S. Zeng, Y. Sheng, O. Yang, Y. B. Chen, Appl. Microbiol. Biotechnol., 85 (2010) 1115–22.

28. M.S.P. Samsom, I. H. Srivatava, J. N. Bright, J. Tate, C.E. Capener, P.C. Biggin, Biochim. Biophys.Acta, 1565(2002) 294-307.

Fig. 1. FTIR spectrum of PANI-ZrPB nanocomposite

Fig. 2. X-ray diffraction pattern of PANI-ZrPB nanocomposite

Fig. 3. FESEM images of a) ZrPB b) PANI-ZrPB and c) EDX of nanocomposite

Fig. 4. TEM images of a) ZrPB b) PANI-ZrPB nanocomposite c) Histogram of size distribution

Fig. 5. TGA/DTA curve of PANI-ZrPB nanocomposite ion exchanger

Fig. 6. (a) Membrane potential values of prepared membrane for different concentration of monovalent and bivalent cations; (b) Transport number for different electrolytes through prepared membrane

Fig. 7. Permselectivity of prepared cation exchange membrane for different concentrations of monovalent and bivalent ionic solutions

Fig. 8. Fixed charge density of prepared membrane for monovalent and bivalent cations

Fig. 9. Growth curves of (a) E.coli (b) Bacillus bacteria in the presence of, control, DMSO, ZrPB, PANI and PANI/ZrPB nanocomposite ion exchanger
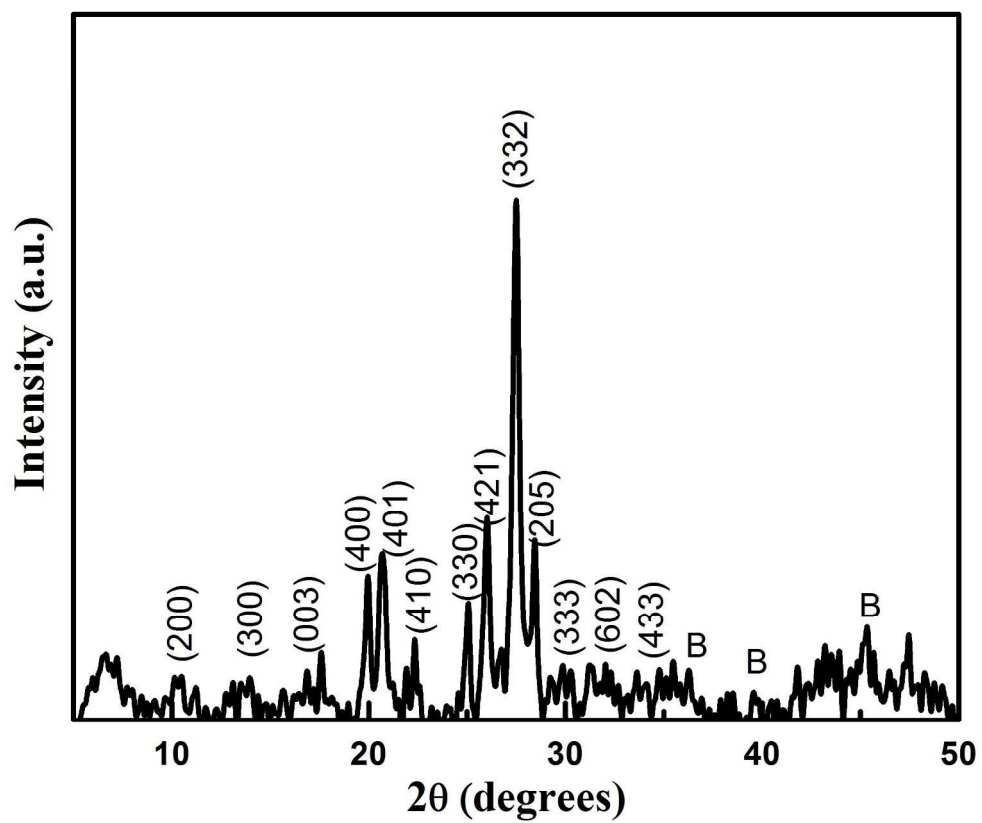
Fig. 10. a) Freundlich adsorption isotherm and; b) Langmuir adsorption isotherm for methylene blue

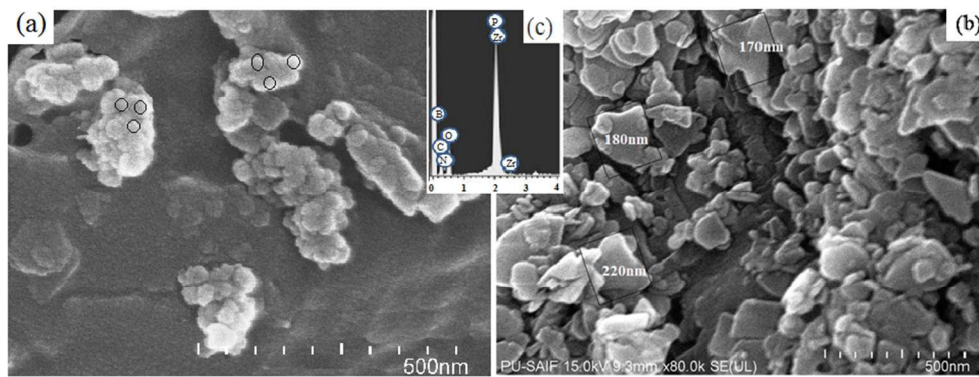Fig. 11. Percentage adsorption and recovery of dye on the nanocomposite
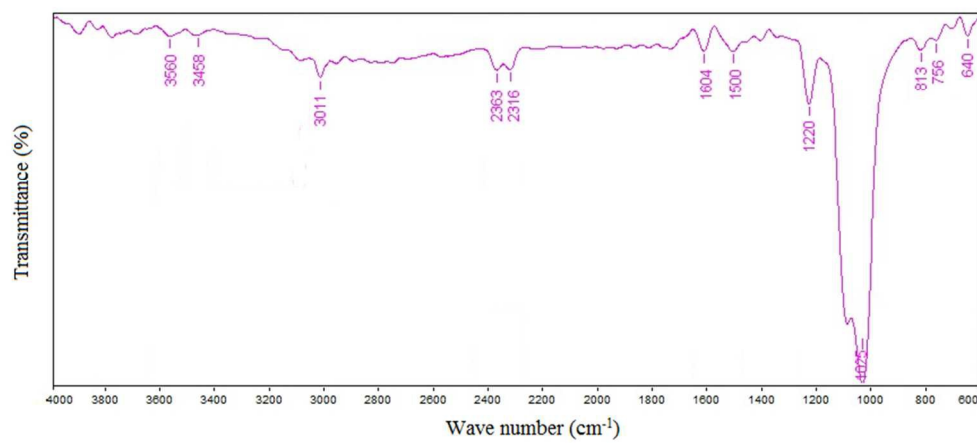
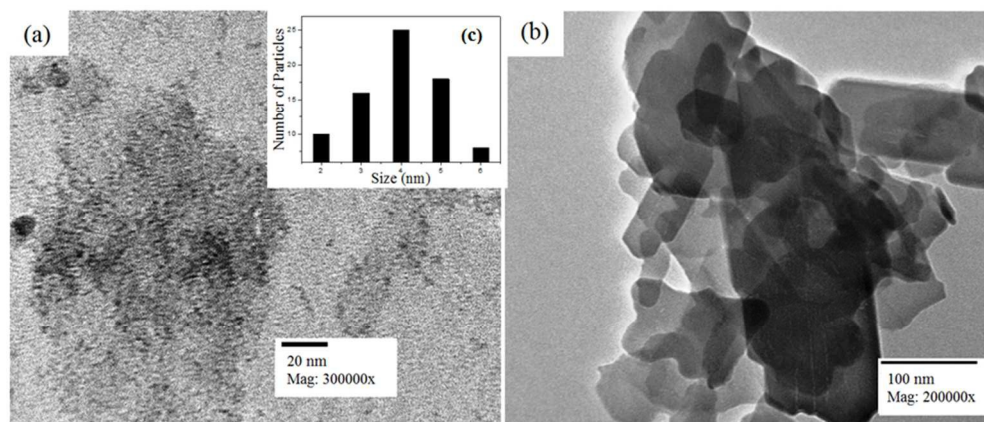FTIR spectrum of PANI-ZrPB nanocomposite

234x106mm (96 x 96 DPI)

X-ray diffraction pattern of PANI-ZrPB nanocomposite
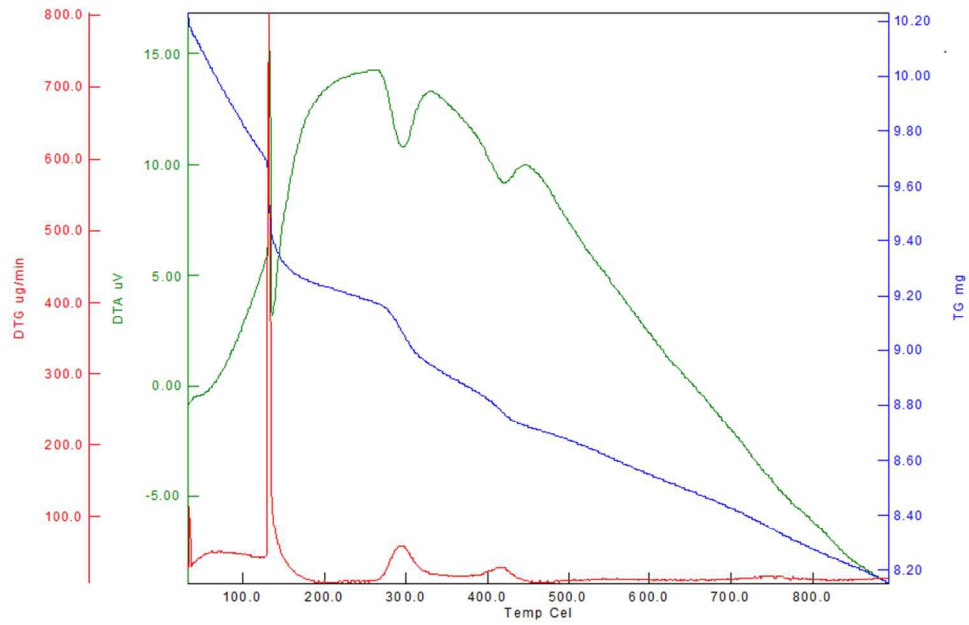
209x176mm (300 x 300 DPI)

FESEM images of a) ZrPB b) PANI-ZrPB and c) EDX of nanocomposite
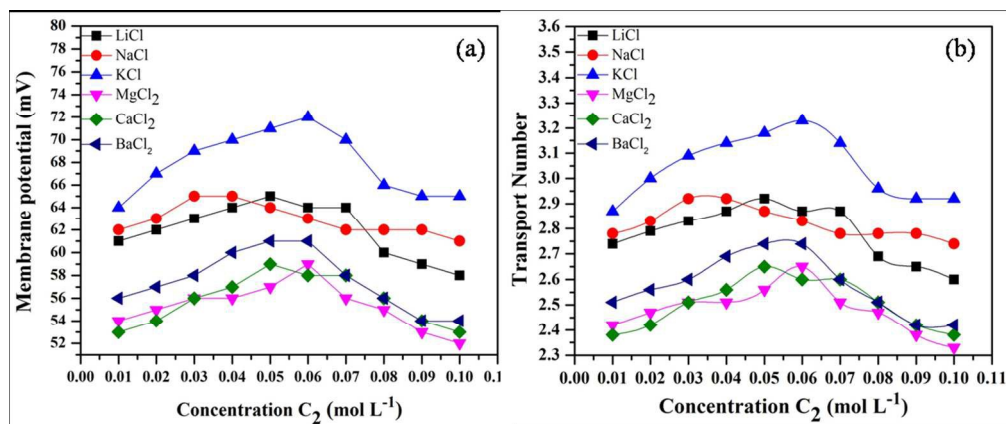
209x79mm (119 x 119 DPI)

TEM images of a) ZrPB b) PANI-ZrPB nanocomposite c) Histogram of size distribution
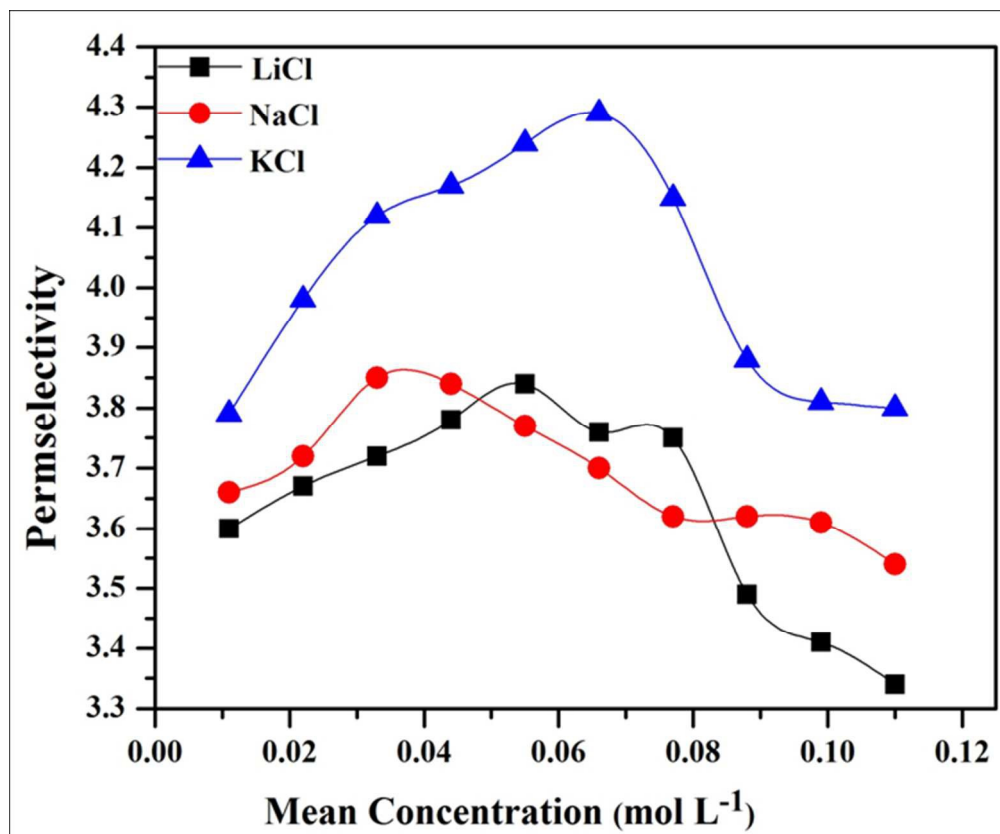
258x110mm (96 x 96 DPI)

TGA/DTA curve of PANI-ZrPB nanocomposite ion exchanger

251x160mm (96 x 96 DPI)

(a) Membrane potential values of prepared membrane for different concentration of monovalent and bivalent cations; (b) Transport number for different electrolytes through prepared membrane
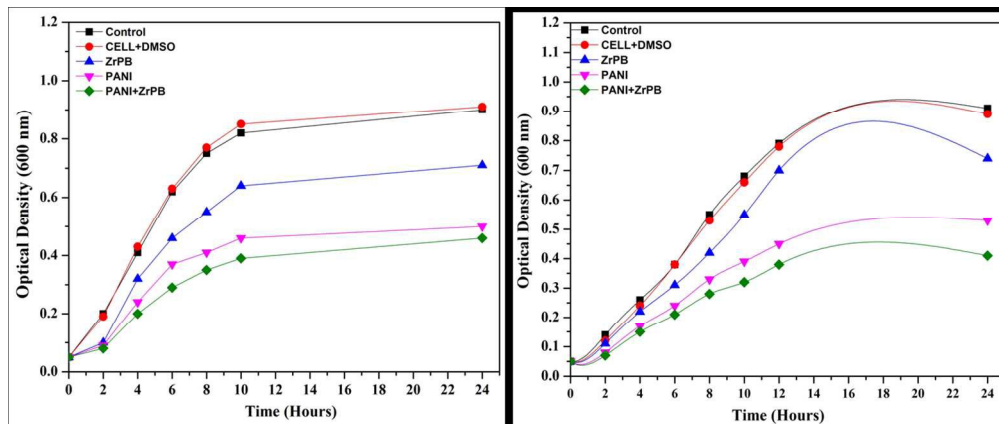
213x89mm (150 x 150 DPI)

Permselectivity of prepared cation exchange membrane for different concentrations of monovalent and bivalent ionic solutions
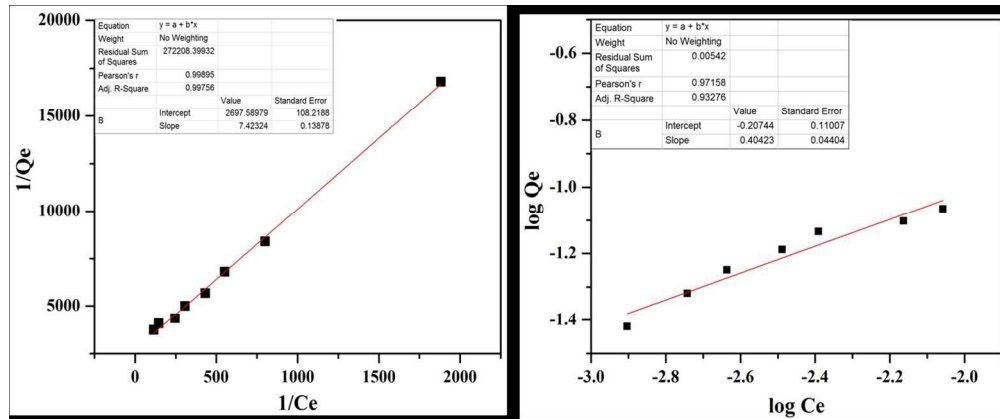
122x101mm (150 x 150 DPI)
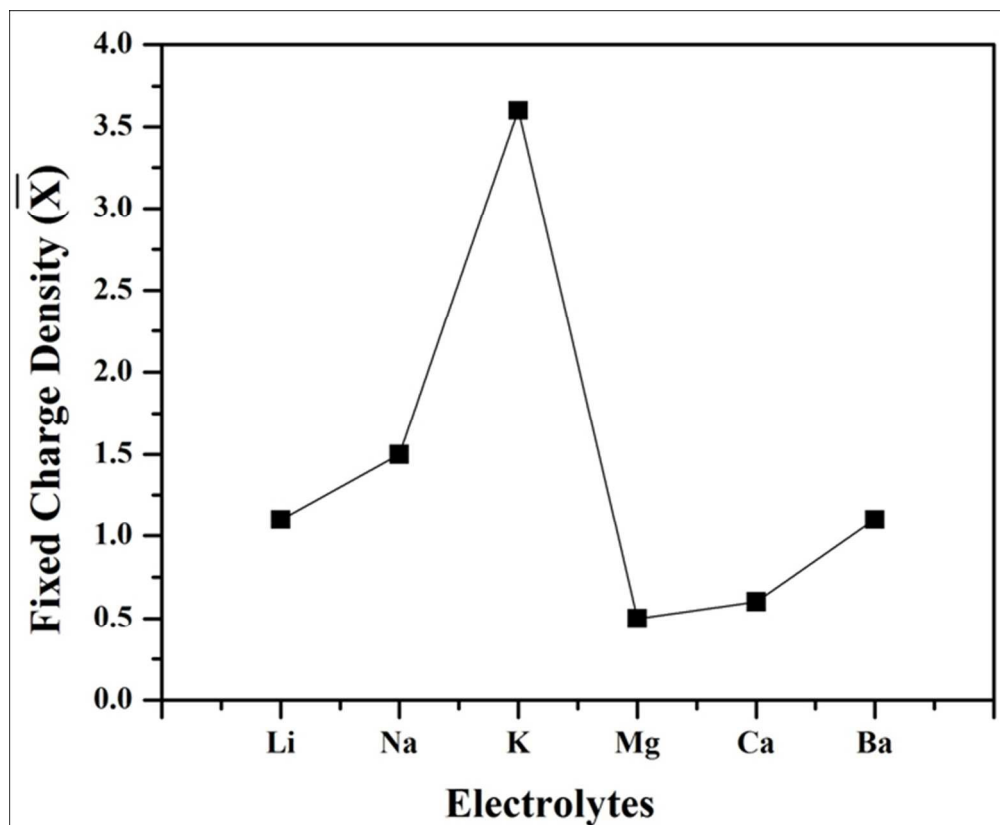
Fixed charge density of prepared membrane for monovalent and bivalent cations

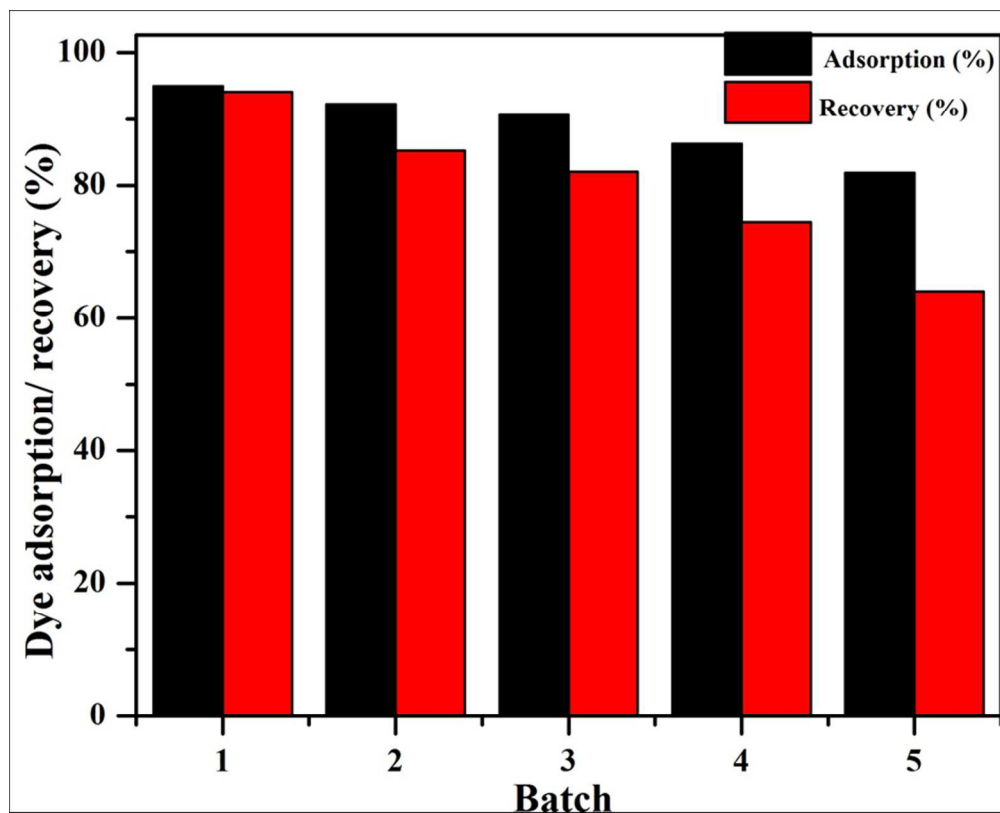124x101mm (150 x 150 DPI)

Growth curves of (a) E.coli (b) Bacillus bacteria in the presence of, control, DMSO, ZrPB, PANI and PANI/ZrPB nanocomposite ion exchanger

256x107mm (150 x 150 DPI)

a) Freundlich adsorption isotherm and; b) Langmuir adsorption isotherm for methylene blue

254x105mm (150 x 150 DPI)

Percentage adsorption and recovery of dye on the nanocomposite

160x128mm (150 x 150 DPI)

Table 1. Optimization of reaction conditions and ion exchange capacity of PANI-ZrPB nanocomposite

| S. No. | Mixing volume ratio (v/v) | | | Mixing volume ratio (v/v) | | Colour | Ion Exchange Capacity (meq g^{-1}) |
	0.1 M zirconyl oxychloride	0.1 M boric acid	0.1 M phosphoric acid	10 % Aniline in 1 M HCl	0.1 M Potassium persulphate		
S-1	1	0.5	0.5	0	0.0	White	0.38
S-2	1	0.5	0.5	0.10	0.10	Green	0.43
S-3	1	0.5	0.5	0.25	0.25	Green	0.51
S-4	1	0.5	0.5	0.50	0.50	Green	0.67
S-5	1	0.5	0.5	1.00	1.00	Green	0.54

Table 2. Physiochemical characteristics of PANI-ZrPB cation exchange membranes

Sample Number	Thickness (mm)	Water Content (%)	Porosity	Na$^+$ ion exchange Capacity (meq/g)
M-1	0.38	11.57	2.4×10^{-2}	0.22
M-2	0.46	7.65	6.3×10^{-3}	0.15
M-3	0.50	5.82	8.4×10^{-3}	0.11

Table 3. Optimisation of pH, adsorbent dosage and contact time for maximum adsorption of methylene blue over nanocomposite surface

S. No.	Dye Conc. (mg/100 ml)	pH[1]	Adsorbent dosage (mg)	Contact time (min)	% Adsorption[2]
1	1.6	3	25	240	6.25
2	1.6	4	25	240	9.3
3	1.6	5	25	240	15.6
4	1.6	6	25	240	19.2
5	1.6	7	25	240	28.9

6	1.6	8	25	240	66.4
7	1.6	9	25	240	83.6
8	1.6	10	25	240	92.3
9	1.6	11	25	240	95.0
10	1.6	11	20	240	93.2
11	1.6	11	15	240	83.1
12	1.6	11	10	240	64.4
13	1.6	11	5	240	39.2
14	1.6	11	20	210	92.5
15	1.6	11	20	180	83.7
16	1.6	11	20	120	66.5
17	1.6	11	20	60	40.1

[1]pH was varied by addition of 1% NaOH; [2]Calculations were made from absorbance measurements using UV spectrophotometer